Journal of Solid State Chemistry 182 (2009) 2491–2496

Contents lists available at ScienceDirect

Journal of Solid State Chemistry

journal homepage: www.elsevier.com/locate/jssc

Synthesis, structure and magnetic behavior of a new three-dimensional Manganese phosphite-oxalate: $[C_2N_2H_{10}][Mn^{II}_2(OH_2)_2(HPO_3)_2(C_2O_4)]$

Padmini Ramaswamy, Sukhendu Mandal, Srinivasan Natarajan *

Framework Solids Laboratory, Solid State and Structural Chemistry Unit, Indian Institute of Science, Bangalore 560 012, India

ARTICLE INFO

Article history:
Received 12 February 2009
Received in revised form
21 June 2009
Accepted 28 June 2009
Available online 2 July 2009

Keywords:
Template synthesis
X-ray diffraction
Hybrid compounds
Manganese
Phosphite

ABSTRACT

A novel manganese phosphite-oxalate, $[C_2N_2H_{10}][Mn^{II}_2(OH_2)_2(HPO_3)_2(C_2O_4)]$ has been hydothermally synthesized and its structure determined by single-crystal X-ray diffraction. The structure consists of neutral manganese phosphite layers, $[Mn(HPO_3)]_\infty$, formed by MnO_6 octahedra and HPO_3 units, cross-linked by the oxalate moieties. The organic cations occupy the middle of the 8-membered one-dimensional channels. Magnetic studies indicate weak antiferromagnetic interactions between the Mn^{2+} ions.

1. Introduction

Open-framework transition metal phosphates have been extensively investigated during the last two decades for their many potential applications in the areas of catalysis, sorption and separation processes [1–3]. It is becoming apparent that the phosphite group, $[HPO_3]^{2-}$, can be employed successfully to replace the traditional phosphate group, $(PO_4)^{3-}$, in some of the open-framework structures. Thus, phosphite analogs of phosphate structures have been prepared and characterized, and phosphite-based structures are beginning to emerge as an important family [4,5]. In addition, it is likely that the reduced number of binding sites in phosphites (three P–O bonds) compared to the phosphates (four P–O bonds) might lead to newer structures in the family of phosphites. Thus, novel phosphite networks have been isolated using Zn [6], Fe [7], V [8] and Cr [9].

It has been shown that the combination of organic and inorganic anions can have considerable potential in forming compounds with open structures. The use of oxalate anions along with phosphates and arsenates has been successfully accomplished, giving rise to a large number of interesting inorganic–organic hybrid structures [2,10–13]. In this context, the use of phosphites and oxalates in conjunction with each other has not been investigated in detail. We have been interested in the study of hybrid structures based on the phosphite and the oxalate moieties, which have given rise to new compounds with novel structures [14,15]. One of the motivating factors for this work is the fact that the average charge per oxygen on the phosphite group (0.66) and the oxalate group (0.50) is less than that on the normally tetrahedral phosphate (0.75), which could lead to interesting structures with unusual metal: phosphite/oxalate ratios. Presently, we have isolated a new three-dimensional manganese phosphite-oxalate compound, $[C_2N_2H_{10}][Mn^{II}_2(OH_2)_2(HPO_3)_2(C_2O_4)]$. The structure has manganese phosphite layers, $[Mn_2(OH)_2(HPO_3)_2]$, connected by the oxalate units. In this paper we report the synthesis, structure, thermal stability and magnetic behavior of the above compound.

2. Experimental

2.1. Synthesis and characterization

The compound was synthesized employing hydrothermal methods. Pale pink plate-like crystals of $[C_2N_2H_{10}][Mn^{II}_2(OH_2)_2(HPO_3)_2(C_2O_4)]$ were obtained from a reaction mixture of $MnCl_2 \cdot 4H_2O$, $H_2C_2O_4 \cdot 2H_2O$, H_3PO_3, ethylenediamine and distilled H_2O with a molar ratio of $1.0MnCl_2 \cdot 4H_2O{:}1.0H_2C_2O_4 \cdot 2H_2O{:}2.0H_3PO_3{:}2.0en{:}122.0H_2O$. In a typical synthesis, 0.629 g of $MnCl_2 \cdot 4H_2O$ was dispersed in 7 mL distilled water. To this 0.401 g of oxalic acid and 0.522 g of H_3PO_3 were added. Finally 0.429 mL of en was added to the reaction mixture and it was stirred to homogeneity (~30 min) at room temperature. This mixture was then sealed in a 23 mL PTFE-lined stainless steel autoclave and heated at 150 °C for 48 h. The initial pH of the

* Corresponding author. Fax: +91 80 2360 1310.
E-mail address: snatarajan@sscu.iisc.ernet.in (S. Natarajan).

0022-4596/$ - see front matter © 2009 Elsevier Inc. All rights reserved.
doi:10.1016/j.jssc.2009.06.040

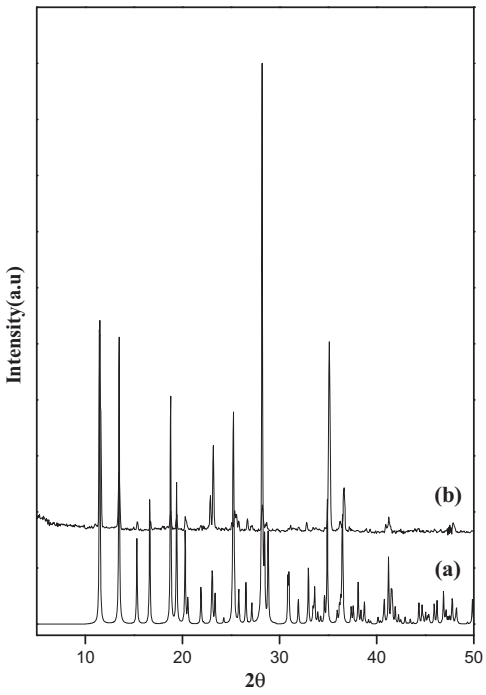

Fig. 1. The powder X-ray diffraction pattern (CuKα) of $[C_2N_2H_{10}][Mn^{II}_2(OH_2)_2(HPO_3)_2(C_2O_4)]$, **I** (a) simulated and (b) experimental.

mixture was 4.0 and there was no observable change in pH during the reaction. The yield of the product was ~60% based on manganese. Elemental analysis showed that the compound contains 10.42, 3.39 and 6.10 wt% of C, H and N, respectively, which is in accordance with the expected values of 10.53, 3.51 and 6.14 wt% of C, H and N on the basis of the empirical formula given by the single-crystal structure analysis.

The initial characterizations were carried out using powder X-ray diffraction (XRD), thermogravimetric analysis (TGA) and infrared (IR) measurements. The powder X-ray diffraction pattern was recorded in the 2θ range 5°–50° using CuKα radiation (Philips, X'pert Pro). The XRD pattern of the bulk product was in good agreement with the simulated XRD pattern generated from the single-crystal structure (Fig. 1).

Thermogravimetric analysis was performed in an atmosphere of flowing oxygen (flow rate = 50 mL/min) in the temperature range 30–800 °C (heating rate = 5 °C/min; Mettler-Toledo, TG850). The results show two separate weight losses (Fig. S1, ESI). The first broad weight loss of 25.4% occurring in the region 150–400 °C corresponds with the loss of the coordinated water and the oxalate moieties (calc.27.3%). The second weight loss of 10.2% occurring in the region of 500–650 °C corresponds to the loss of the amine molecules (calc.13.6%). The final product, after the TGA studies, was identified by powder XRD as $Mn_2P_2O_7$ (JCPDS: 35–1497). The calculated weight loss due to the loss of the water molecules and the decomposition of the organic amine and the oxalate moiety is 40.8%, but the observed weight loss was only 35.6%. This difference in the observed and calculated weight loss can be explained by considering the weight gained due to the oxidation of P(III) to P(V) (~7.0%). Thus, the total weight loss would be 42.6% (35.6+7.0), which is much closer to the expected calculated weight loss of 40.8%. The TGA behavior can be understood as follows:

$$[C_2N_2H_{10}][Mn_2(OH_2)_2(HPO_3)_2(C_2O_4)]+7.5O_2 = Mn_2P_2O_7(s)+4CO_2(g)\uparrow+8H_2O(g)\uparrow+2NO_2(g)\uparrow$$

Table 1
Crystal data and structure refinement parameters for $[C_2N_2H_{10}][Mn^{II}_2(OH_2)_2(HPO_3)_2(C_2O_4)]$, **I**.

Empirical formula	$C_2H_8NO_6PMn$
Formula weight	227.883
Crystal system	Monoclinic
Space group	P2(1)/c
a (Å)	7.8371 (14)
b (Å)	8.7545 (15)
c (Å)	10.1003 (18)
β (deg.)	100.605 (3)
Volume (Å^3)	681.1 (2)
Z	4
T (K)	293
ρ_{calc} (g cm^{-3})	2.223
μ (mm^{-1})	2.157
θ range (deg)	2.64–27.98
λ (Mo Kα) (Å)	0.71073
Reflections collected	5643
Unique reflections	1589
Number of parameters	108
Goodness of fit (S)	1.081
R indexes [$I>2\sigma(I)$]	$R_1 = 0.0360$, $wR_2 = 0.1030$
R (all data)	$R_1 = 0.0366$, $wR_2 = 0.1036$
Largest diff. peak and hole eÅ^{-3}	3.042 and −0.489

$R_1 = \sum||F_o|-|F_c||/\sum|F_o|$; $wR_2 = \{\sum[w(F_o^2-F_c^2)]/\sum[w(F_o^2)^2]\}^{1/2}$. $w = 1/[\rho^2(F_o)^2+(aP)^2+bP]$.
$P = [\max(F_o, O)+2(F_c)^2]/3$, where $a = 0.0625$ and $b = 1.3773$.

IR spectroscopic studies were carried out in the mid-IR range 400–4000 cm^{-1} using the KBr pellet method (Perkin Elmer, SPECTRUM 1000). The IR spectrum of $[C_2N_2H_{10}][Mn^{II}_2(OH_2)_2(HPO_3)_2(C_2O_4)]$ showed the characteristic bands of the protonated ethylenediamine molecule, the HPO_3 unit and the C_2O_4 moieties (Fig. S2, ESI). The observed IR bands are: $\nu(PO_3) = 1071$ cm^{-1}, $\delta_s(PO_3) = 595$ cm^{-1}, $\delta_{as}(PO_3) = 497$ cm^{-1}, ν(P–H) = 2346 cm^{-1}, $\nu(H_2O) = 3487$ cm^{-1}, ν(N–H) = 3295 cm^{-1}, ν(C–H) = 3100 cm^{-1}, ν(C–C) = 1626 cm^{-1}, ν_s(C–O) = 1319 cm^{-1}, ν_{as}(C–O) = 1627 cm^{-1}.

The temperature variation of the magnetic behavior was investigated on the powdered sample in the range 4–300 K with a SQUID magnetometer (Quantum Design Inc., USA).

2.2. Single-crystal X-ray diffraction

A suitable colorless single crystal of the compound was carefully selected under a polarizing microscope and glued to a thin glass fiber. The single-crystal X-ray diffraction data were collected on a Bruker AXS Smart Apex CCD diffractometer at room temperature (293 K). The X-ray generator was operated at 50 kV and 35 mA using Mo Kα ($\lambda = 0.71073$ Å) radiation. Data were collected with ω scans of width 0.3°. A total of 606 frames were collected in three different settings of φ (0, 90 and 180°), keeping the sample-to-detector distance fixed at 6 cm and the detector position fixed at −25°. Pertinent experimental details of the structure determination are listed in Table 1.

The data were reduced using SAINTPLUS [16] and an empirical absorption correction was applied using the SADABS program [17]. The crystal structure was solved and refined by direct methods using SHELXL-97 present in the WinGx suite of program [18]. The hydrogen positions for the atoms were placed in geometrically ideal positions and refined using the riding mode. The last cycles of refinements included all the atomic positions, anisotropic thermal parameters for all the non-hydrogen atoms and isotropic thermal parameters for all the hydrogen atoms. Full-matrix-least-squares structure refinement against $|F|^2$ was carried out using the WinGx suite of program [18]. CCDC 715030 contains the supplementary crystallographic data (CIF file) for the above compound. The data can be obtained free of charge from The

Cambridge Crystallographic Data Centre via www.ccdc.cam.ac.uk/data_request/cif.

3. Results and discussion

3.1. Structure of $[C_2N_2H_{10}][Mn^{II}_2(OH_2)_2(HPO_3)_2(C_2O_4)]$, **I**

The asymmetric unit of **I** contains 11 non-hydrogen atoms, of which one Mn and one P atoms are crystallographically independent (Fig. 2(a)). The manganese atom is octahedrally coordinated by six oxygen atoms with an average Mn–O bond distance of 2.19 Å. Three types of Mn–O bonds are present: three Mn–O–P, two Mn–O–C and one Mn–O_{water}, with the bond angles and lengths being in the expected range. The phosphorous atom is connected to the manganese atom through three Mn–O–P bonds and possesses one P–H bond. The P–O bond distances have an average value of 1.522 Å and an average O–P–O bond angle of 112.78°. Bond valence sum calculations indicate that one of the oxygen atoms [(O(6)] is a water molecule. Selected bond distances and angles are listed in Table 2.

The structure consists of a network of MnO_6 octahedra, HPO_3 pseudotetrahedra and the oxalate units. The strictly alternating MnO_6 and HPO_3 units are connected through their vertices to form neutral $MnHPO_3$ two-dimensional layers with 4- and 8-membered apertures in the *bc* plane (Fig. 2(b)). The oxalate units link the Mn centers from two different layers, giving rise to an anionic three-dimensional structure, $[C_2N_2H_{10}][Mn^{II}_2(OH_2)_2$

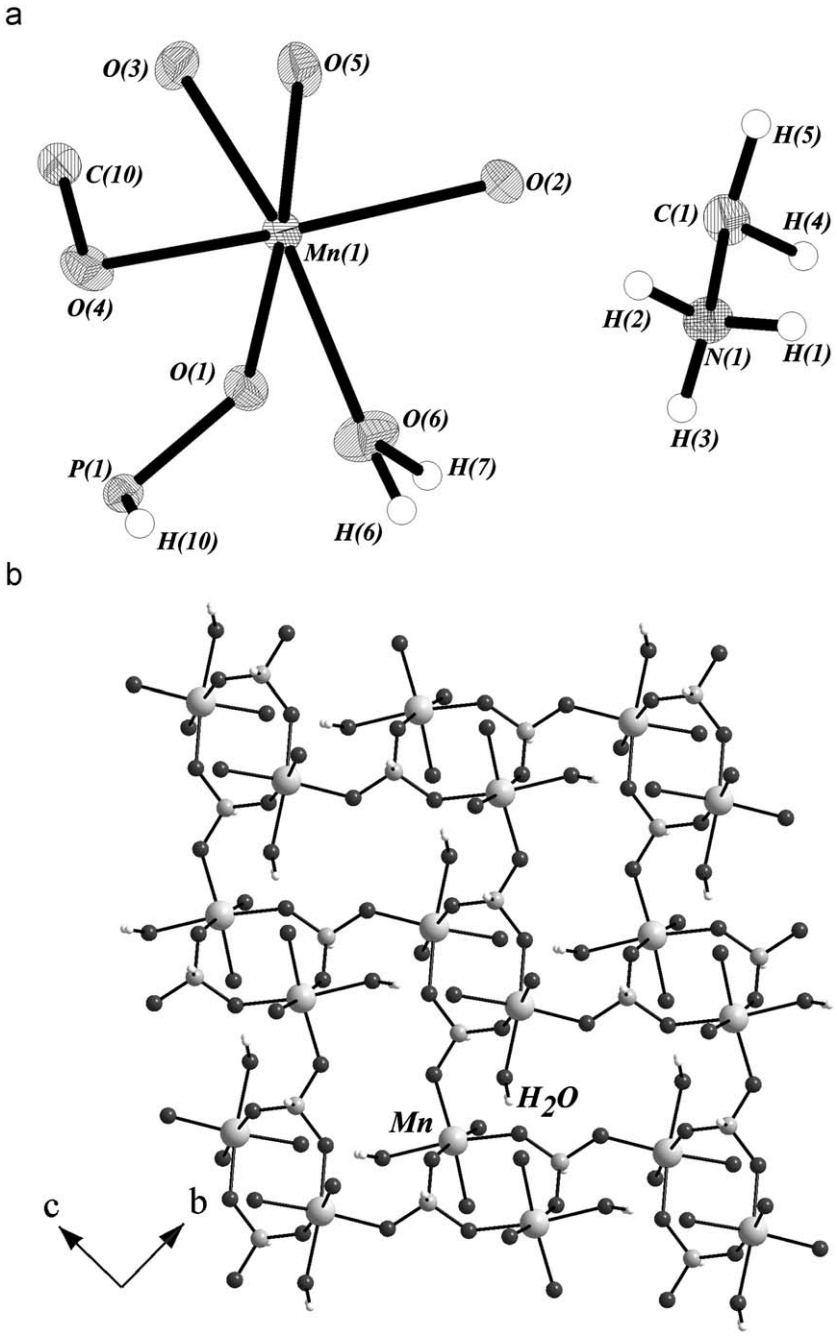

Fig. 2. (a) The asymmetric unit of $[C_2N_2H_{10}][Mn^{II}_2(OH_2)_2(HPO_3)_2(C_2O_4)]$, **I**. Thermal ellipsoids are shown at 50% probability. (b) View of the manganese phosphite, $[Mn(HPO_3)]_\infty$ layers in **I** in the *bc* plane. Note the presence of 4- and 8-membered rings in the layers.

Table 2
Selected bond distances and angles in $[C_2N_2H_{10}][Mn^{II}_2(OH_2)_2(HPO_3)_2(C_2O_4)]$, **I**.

Bond	Distance (Å)	Bond	Distance (Å)
Mn(1)–O(1)	2.109 (2)	P(1)–O(2)#2	1.526 (2)
Mn(1)–O(2)	2.118 (2)	P(1)–O(3)#1	1.520 (2)
Mn(1)–O(3)	2.138 (2)	O(4)–C(10)	1.256 (3)
Mn(1)–O(4)	2.237 (2)	O(5)–C(10)#4	1.240 (3)
Mn(1)–O(5)	2.266 (2)	C(10)–C(10)#4	1.561 (5)
Mn(1)–O(6)	2.290 (2)	N(1)–C(1)	1.488 (3)
P(1)–O(1)	1.520 (2)	C(1)–C(1)#5	1.509 (5)
Angle	**Amplitude (°)**	**Angle**	**Amplitude (°)**
O(1)–Mn(1)–O(2)	98.30 (8)	O(5)–Mn(1)–O(6)	99.49 (8)
O(1)–Mn(1)–O(3)	91.74 (8)	O(3)#1–P(1)–O(1)	114.34 (11)
O(2)–Mn(1)–O(3)	99.10 (8)	O(3)#1–P(1)–O(2)#2	110.48 (11)
O(1)–Mn(1)–O(4)	101.19 (7)	O(1)–P(1)–O(2)#2	113.52 (11)
O(2)–Mn(1)–O(4)	156.73 (8)	P(1)–O(1)–Mn(1)	134.82 (12)
O(3)–Mn(1)–O(4)	92.92 (8)	P(1)#3–O(2)–Mn(1)	130.36 (11)
O(1)–Mn(1)–O(5)	174.56 (7)	P(1)#1–O(3)–Mn(1)	134.15 (12)
O(2)–Mn(1)–O(5)	87.13 (7)	C(10)–O(4)–Mn(1)	114.60 (16)
O(3)–Mn(1)–O(5)	87.69 (8)	C(10)#4–O(5)–Mn(1)	113.86 (16)
O(4)–Mn(1)–O(5)	73.45 (7)	O(5)#4–C(10)–O(4)	126.0 (2)
O(1)–Mn(1)–O(6)	80.51 (8)	O(5)#4–C(10)–C(10)#4	117.4 (3)
O(2)–Mn(1)–O(6)	87.72 (8)	O(4)–C(10)–C(10)#4	116.6 (3)
O(3)–Mn(1)–O(6)	170.39 (8)	N(1)–C(1)–C(1)#5	111.3 (3)
O(4)–Mn(1)–O(6)	83.11 (8)		

Symmetry transformations used to generate equivalent atoms: #1 $-x+1$, $-y+1$, $-z$#2 $-x+1$, $y+1/2$, $-z+1/2$ #3 $-x+1$, $y-1/2$, $-z+1/2$ #4 $-x$, $-y+1$, $-z$ #5 $-x$, $-y+1$, $-z+1$.

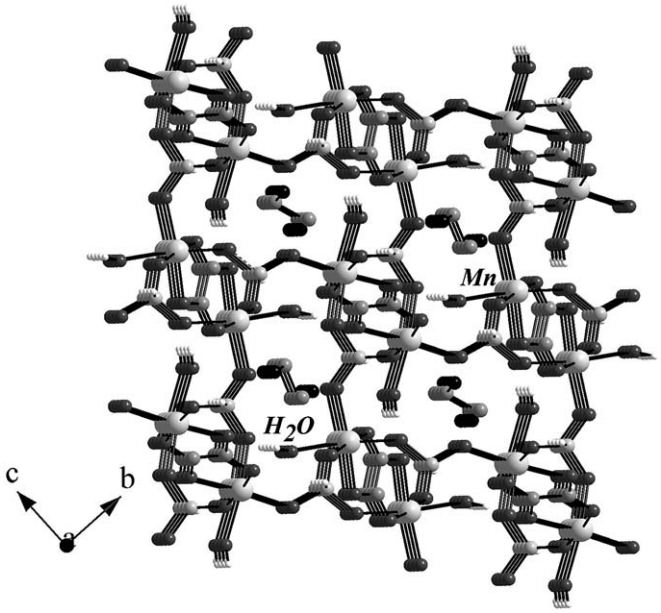

Fig. 3. Structure of **I** along the *a* axis, showing the one-dimensional channels. Note that the amine molecules occupy the middle of the channels. Hydrogen atoms on the amine molecule are not shown for clarity.

$(HPO_3)_2(C_2O_4)]$, possessing 8-membered one-dimensional channels. Charge neutrality is achieved by the presence of protonated ethylenediamine molecules, which occupy the middle of the 8-membered one-dimensional channels (Fig. 3). The terminal bonded water molecules also project into the 8-membered channel. The close proximity of the ethylenediammonium cations, framework oxygens and the water molecules give rise to hydrogen bond interactions (Fig. S3, ESI). Thus, O–H…O, N–H…O and C–H…O interactions have been observed. The important hydrogen bond interactions are observed in Table 3.

In the structure of **I**, the manganese phosphite layers are formed by 4- and 8-membered apertures, and are purely inorganic and neutral. These layers are cross-linked in an *out-of-plane*

Table 3
Important observed hydrogen bond interactions in $[C_2N_2H_{10}][Mn^{II}_2(OH_2)_2(HPO_3)_2(C_2O_4)]$, **I**.

D–H…A	D–H (Å)	H…A (Å)	D…A (Å)	D–H…A (Å)
N(1)–H(1)…O(1)	0.89	1.90	2.782 (3)	172
N(1)–H(2)…O(2)	0.89	2.05	2.929 (3)	171
N(1)–H(3)…O(4)	0.89	2.24	3.100 (3)	162
O(6)–H(6)…O(3)	0.94	1.86	2.797 (3)	176
O(6)–H(7)…O(4)	0.95	1.94	2.871 (3)	167
C(1)–H(4)…O(5)	0.97	2.38	3.342 (4)	170
C(1)–H(5)…O(5)	0.97	2.46	3.404 (3)	164

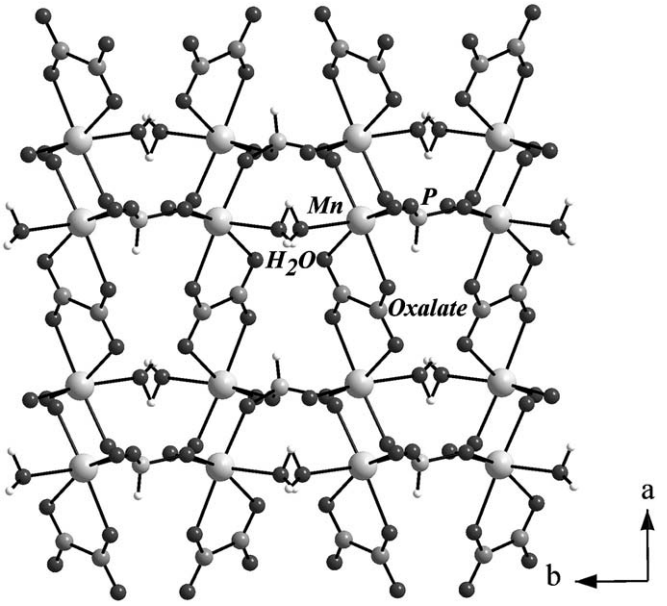

Fig. 4. View of the layers in **I** connected by oxalate units.

fashion by the oxalate units (Fig. 4). Similar inorganic layers pillared by the oxalate units have been observed in the iron-based inorganic–organic hybrid systems, $[Fe_2(OH_2)_2(HPO_4)_2(C_2O_4)]\cdot 2H_2O$ [11] and $[C_2N_2H_{10}][Fe^{II}_2(OH_2)_2(HPO_3)_2(C_2O_4)]$ [14].

In the light of this, one can compare the structural features of the present compound with other similar structures known in the literature. Since manganese phosphite layers are present, one can make meaningful comparisons with other layered phosphite structures. The formation of layered structures has been frequently observed in the family of open-framework zinc phosphites, which are formed by the vertex connectivity between tetrahedral ZnO_4 and HPO_3 units. Thus, in the zinc phosphites, $[C_2N_2H_{10}][Zn_2(HPO_3)_3]$ [19] and $[(C_4N_2H_{12})(C_5NH_4)]_4[Zn_6(HPO_3)_8]\cdot 2H_2O$ [20], the layers are formed with 4- and 8-membered apertures, just like in the present compound. In the zinc phosphite structures, the 8-membered apertures share edges and are separated by 4-membered rings (Fig. 5(a) and (b)). In $[C_3NH_{10}]_2[Zn_3(HPO_3)_4]$ [20], the connectivity within the layer is comparable to the present structure (Fig. 5(c) and (d)), though the zinc phosphite has a three-dimensional structure. In the present structure, the 4-membered rings appear to be distorted, which may be due to the *out-of-plane* connectivity by the oxalate units.

The presence of 4- and 8-membered rings has also been observed in vanadium phosphite structures. The present structure has close resemblance to the vanadium phosphite, $(VO)_4(4,4'\text{-bpy})_2(HPO_3)_4$ [21]. In the latter, the layers contain 4- and 8-membered apertures formed by the connectivity between VO_4N

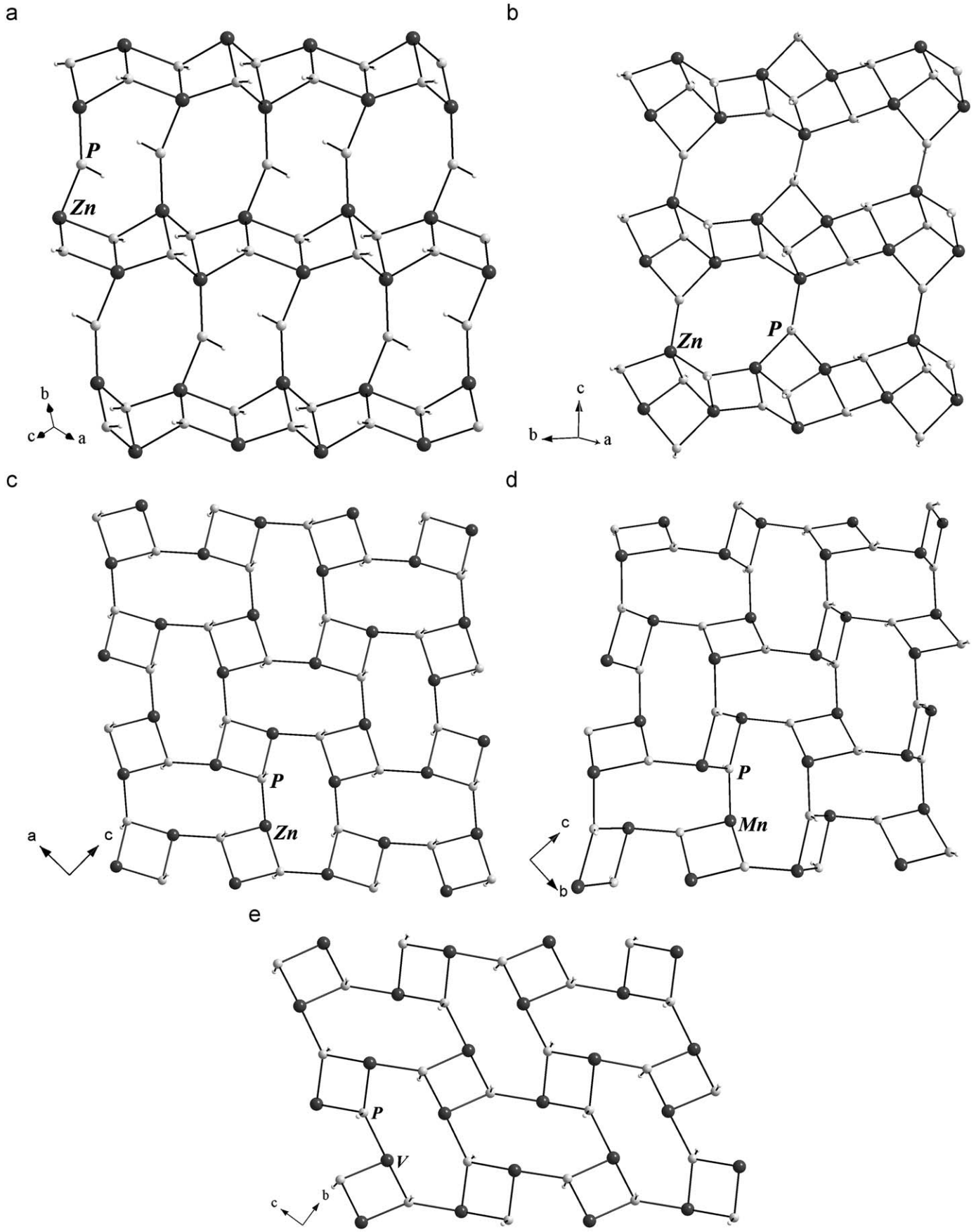

Fig. 5. (a) View of the T-atom (T = Zn, P) connectivity within the layer in the zinc phosphite, $[C_2N_2H_{10}][Zn_2(HPO_3)_3]$, (Ref. [19]). (b) View of the T-atom (T = Zn, P) connectivity within the layer in the zinc phosphite, $[(C_4N_2H_{12})(C_5NH_4)]_4[Zn_6(HPO_3)_8]$, (Ref. [20]). (c) View of the T-atom (T = Zn, P) connectivity within the layer in the three-dimensional zinc phosphite, $[C_3NH_{10}]_2[Zn_3(HPO_3)_4]$, (Ref. [20]). (d) T-atom (T = Mn, P) connectivity in **I** within the layer. Note the close similarity with the zinc phosphite structure (c). (e) View of the T-atom (T = V, P) connectivity within the layer in the three-dimensional vanadium phosphite, $(VO)_4(4,4'\text{-bpy})_2(HPO_3)_4$, (Ref. [21]).

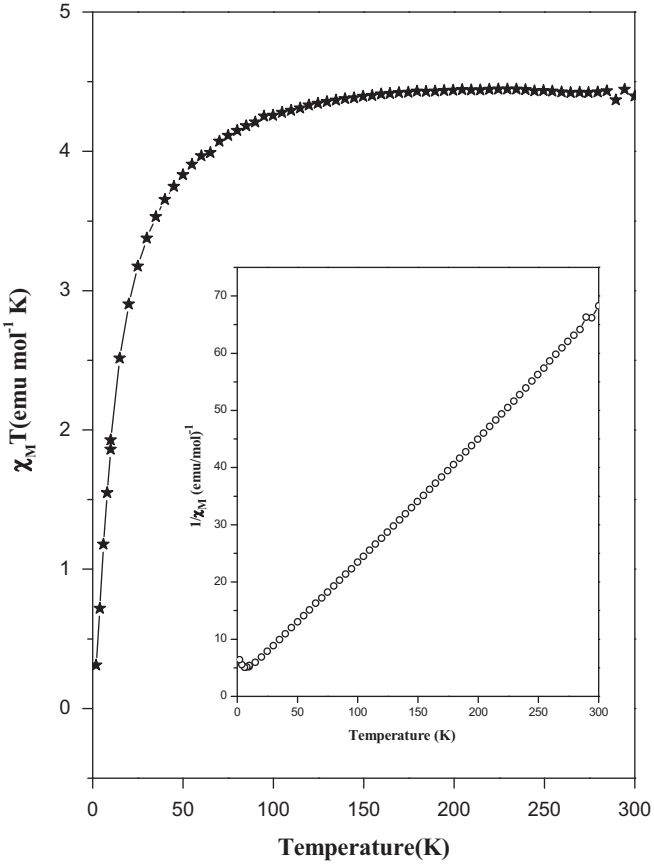

Fig. 6. Temperature dependence of $\chi_m T$ for $[C_2N_2H_{10}][Mn^{II}_2(OH_2)_2(HPO_3)_2(C_2O_4)]$, **I**. Inset shows the inverse of susceptibility as a function of temperature.

trigonal bipyramidal units and the HPO_3 units (Fig. 5(e)). These layers are cross-linked by the 4,4′-bipyridine ligands, giving rise to a three-dimensional structure. In the present compound the $[Mn(HPO_3)_\infty]$ layers are connected by the oxalate moieties to generate a three-dimensional framework.

Though manganese phosphate-oxalate compounds have been synthesized and characterized [12,22], there is only one report of a manganese phosphite-oxalate phase in the literature, $[C_4N_2H_{12}][Mn^{II}_2(HPO_3)_2(C_2O_4)]$ [15]. In this compound, MnO_6 octahedra share edges to form Mn_2O_{10} dimer units, which are connected by the HPO_3 units, forming neutral two-dimensional $[Mn(HPO_3)]_\infty$ layers with 8-membered apertures. In the present compound, we have MnO_6 octahedra connected by HPO_3 units forming $[Mn(HPO_3)]_\infty$ layers with 4- and 8-membered apertures. In both the cases, the oxalate moieties connect the layers giving rise to the observed three-dimensional structures.

3.2. Magnetic susceptibility

The variable temperature magnetic susceptibility studies were carried out in the range 300–2 K. At room temperature, the observed effective magnetic moment (μ_{eff}) per Mn^{2+} ion is 5.95 μ_B, which is in good agreement with the spin-only value of Mn^{II} in the high-spin state (5.92 μ_B). The $\chi_m T$ versus T curve is shown in Fig. 6. The $\chi_m T$ value decreases continuously and reaches a minimum of 0.311 emu mol^{-1} K at 2 K. The $1/\chi_m$ versus T curve is shown as the inset of Fig. 6. Above 50 K, the magnetic behavior can be fitted by the Curie–Weiss law $\chi_m = Cm/(T-\theta)$ (χ_m is the measured magnetic susceptibility, T the temperature (K), Cm the Curie constant and θ the Weiss constant), with $Cm = 4.49\,cm^3K/mol$ and $\theta_p = -3.47$ K. The negative and small θ_p value indicates that the magnetic interactions between the Mn centers are antiferromagnetic, but weak. Similar antiferromagnetic behavior has been observed earlier in many organic–inorganic hybrid compounds [11,14].

In conclusion, a new three-dimensional inorganic–organic hybrid phosphite–oxalate phase of manganese has been synthesized and characterized. The magnetic studies indicate antiferromagnetic behavior. Though the present compound has close similarities to the phosphate–oxalate structure reported earlier [11], the isolation of inorganic–organic structures based on phosphites is important as such structures are not many in the literature. The synthesis of phosphite–oxalate structures of many different elements clearly indicates that the structural and compositional diversity of these compounds is also rich and can be compared well with the family of phosphate–oxalate hybrid structures.

Acknowledgments

S.N thanks the Department of Science and Technology (DST) and the Council of Scientific and Industrial Research (CSIR), Government of India, for the award of a research grant. S.N also thanks the Department of Science and Technology (DST), Government of India, for the award of a RAMANNA fellowship.

Appendix A. Supporting Information

Supplementary data associated with this article can be found in the online version at doi:10.1016/j.jssc.2009.06.040.

References

[1] A.K. Cheetham, T. Loiseau, G. Ferey, Angew. Chem. Int. Ed. 38 (1999) 3268.
[2] S. Natarajan, S. Mandal, Angew. Chem. Int. Ed. 47 (2008) 4798.
[3] D. Maspoch, D.-R. Molina, J. Veciana, Chem. Soc. Rev. 36 (2007) 770.
[4] J.A. Rodgers, W.T.A. Harrison, Chem. Commun. 23 (2000) 2385.
[5] S.F. Armas, J.L. Mesa, J.L. Pizarro, U.-C. Chung, M.I. Arriortua, T. Rojo, J. Solid State Chem. 178 (2005) 3554.
[6] L.E. Gordon, W.T.A. Harrison, Inorg. Chem. 43 (2004) 1808; S. Mandal, S. Natarajan, Inorg. Chem. 47 (2008) 5304.
[7] U.-C. Chung, J.L. Mesa, J.L. Pizarro, J.R. Fernandez, J.S. Marcos, J.S. Garitaonandia, M.I. Arriortua, T. Rojo, Inorg. Chem. 45 (2006) 8965.
[8] S. Fernandez, J.L. Mesa, J.L. Pizarro, L. Lezama, M.I. Arriortua, T. Rojo, Chem. Mater. 14 (2002) 2300.
[9] S. Fernandez, J.L. Mesa, J.L. Pizarro, L. Lezama, M.I. Arriortua, T. Rojo, Angew. Chem. Int. Ed. 41 (2002) 3683.
[10] S. Chakrabarti, M.A. Green, S. Natarajan, Solid State Sci. 4 (2002) 405.
[11] H. Meng, G.-H. Li, Y. Xing, Y.-L. Yang, Y.-J. Cui, L. Liu, H. Ding, W.-Q. Pang, Polyhedron 23 (2004) 2357.
[12] Z.A.D. Lethbridge, S.K. Tiwary, A. Harrison, P. Lightfoot, J. Chem. Soc., Dalton Trans. 12 (2001) 1904.
[13] K. Kedarnath, A. Choudhury, S. Natarajan, J. Solid State Chem. 150 (2000) 324.
[14] S. Mandal, S. Natarajan, Chem. Eur. J. 13 (2007) 968.
[15] S. Mandal, M.A. Green, S.K. Pati, S. Natarajan, J. Mater. Chem. 17 (2007) 980.
[16] SMART (V 5.628), SAINT (V 6.45a), XPREP and SADABS, Bruker AXS Inc. Madison, Wisconsin, USA, 2004.
[17] G.M. Sheldrick, SADABS Siemens Area Detector Absorption Correction Program, University of Göttingen, Göttingen, Germany, 1994.
[18] WinGx V 1.64.05, Crystallograhic Program for Windows, 2003.
[19] Z.-E. Lin, J. Zhang, S.-T. Zheng, G.-Y. Yang, Solid State Sci. 6 (2004) 371.
[20] S. Mandal, S. Natarajan, Solid State Sci. 8 (2006) 388.
[21] Z. Shi, G. Li, D. Zhang, J. Hua, S. Feng, Inorg. Chem. 42 (2003) 2357.
[22] R. Yu, X. Xing, T. Saito, M. Azuma, M. Takano, D. Wang, Y. Chen, N. Kumada, N. Kinomura, Solid State Sci. 7 (2005) 221.